Journal of Environmental Monitoring

Cutting-Edge Research on Environmental Processes & Impacts
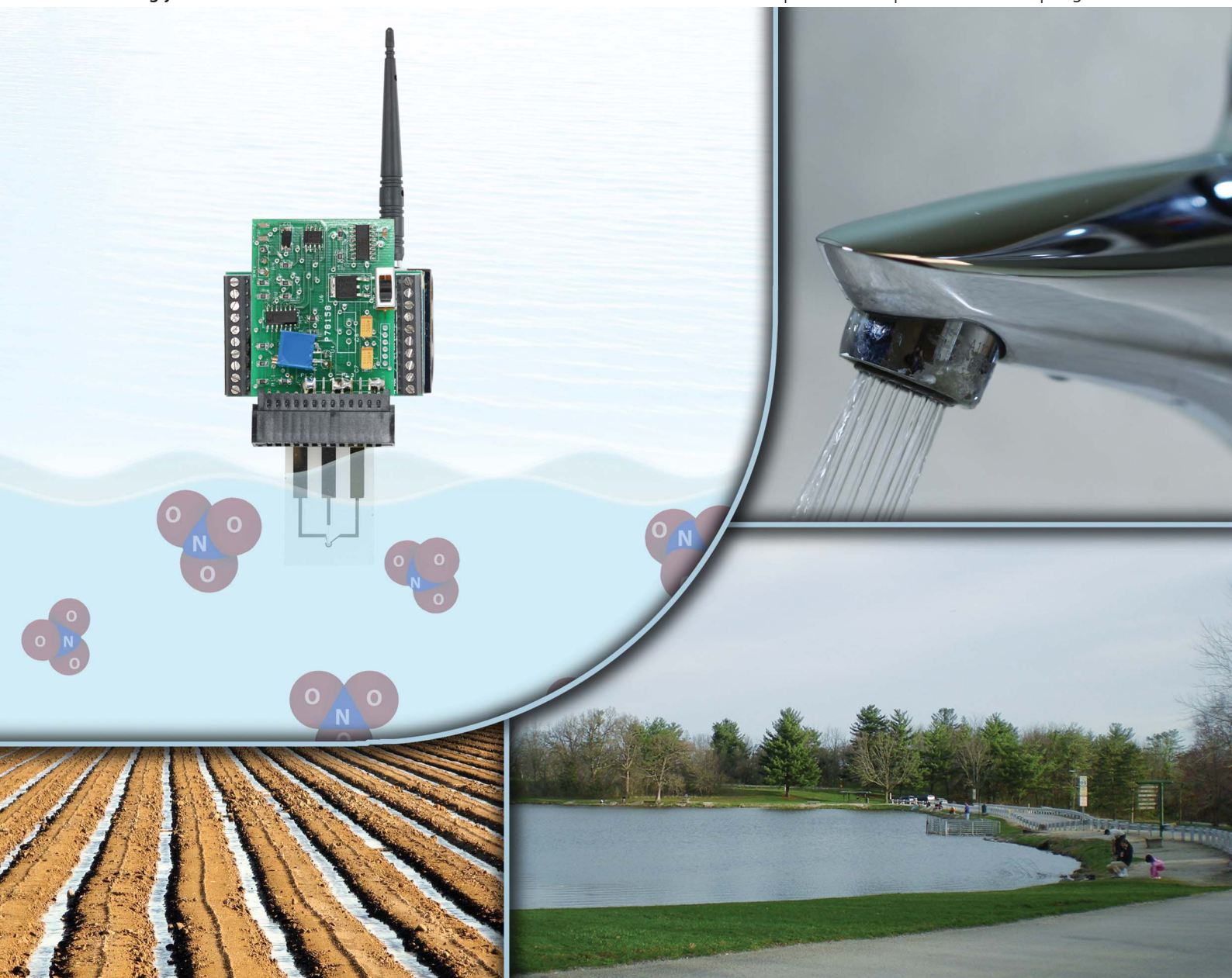
RSCPublishing

PAPER
Gang Logan Liu *et al.*
The microelectronic wireless nitrate sensor network for environmental water monitoring

Dynamic Article Links ▶

PAPER

The microelectronic wireless nitrate sensor network for environmental water monitoring†

Manas Ranjan Gartia,[ab] Björn Braunschweig,[c] Te-Wei Chang,[bd] Parya Moinzadeh,[e] Barbara S. Minsker,[f] Gul Agha,[e] Andrzej Wieckowski,[g] Laura L. Keefer[h] and Gang Logan Liu*[bd]

Quantitative monitoring of water conditions in a field is a critical ability for environmental science studies. We report the design, fabrication and testing of a low cost, miniaturized and sensitive electrochemical based nitrate sensor for quantitative determination of nitrate concentrations in water samples. We have presented detailed analysis for the nitrate detection results using the miniaturized sensor. We have also demonstrated the integration of the sensor to a wireless network and carried out field water testing using the sensor. We envision that the field implementation of the wireless water sensor network will enable "smart farming" and "smart environmental monitoring".

Introduction

Nitrogen is not only an essential plant nutrient but also an important building block of life and as such nitrogen is contained in nucleotides, amino acids, and proteins.[1] The ubiquitous presence of nitrate ion is fostered due to its high solubility in water. Due to industrial pollution, nitrate leaching from aerated soils, excessive use of fertilizers and animal wastes,[2–7] nitrate may build up in freshwater and marine aquatic ecosystems that can

[a]Department of Nuclear, Plasma and Radiological Engineering, University of Illinois, Urbana-Champaign, Urbana, IL 61801, USA

[b]Micro and Nanotechnology Laboratory, University of Illinois, Urbana-Champaign, Urbana, IL 61801, USA. E-mail: loganliu@illinois.edu

[c]Institute of Particle Technology, University of Erlangen-Nuremberg, Erlangen 91058, Germany

[d]Department of Electrical and Computer Engineering, University of Illinois, Urbana-Champaign, Urbana, IL 61801, USA

[e]Department of Computer Science, University of Illinois, Urbana-Champaign, Urbana, IL 61801, USA

[f]Civil and Environmental Engineering, University of Illinois, Urbana-Champaign, Urbana, IL 61801, USA

[g]Department of Chemistry, University of Illinois, Urbana-Champaign, Urbana, IL 61801, USA

[h]Illinois State Water Survey, Prairie Research Institute, University of Illinois, Urbana-Champaign, Urbana, IL 61801, USA

† Electronic supplementary information (ESI) available. See DOI: 10.1039/c2em30380a

lead to algal blooms and eutrophication.[8] For these reasons, the U.S. Environmental Protection Agency (EPA) has set the maximum allowable contaminant levels (MCL) for nitrate-nitrogen as 10 ppm (10 mg L^{-1} or 0.7 mM) and for nitrite-nitrogen as 1 ppm (1 mg L^{-1}).[9]

Nitrate concentrations in soil and water fluctuate, both spatially and temporally,[10] depending on the season, weather conditions and locality. Nitrate concentrations in soil solutions have been reported[11,12] to vary from a few hundred micromolars to around 20 millimolars, with the highest concentration of 70 millimolars.[1] By developing methods to understand the nitrous uptake in a field at fine spatial and temporal granularity, fields could be instrumented to minimize such run-offs.

Currently most environmental observations are under sampled due to logistics involved in sample analysis and this may create a bias in characterizing the dominant seasonal, daily, or semi-diurnal processes.[13] Therefore, in order to understand the variability driven by natural and anthropogenic climate change, long-term high frequency monitoring of the environment is necessary.[13] The same monitoring system, the nitrate sensor network in our case, can be utilized for monitoring drinking water quality, wastewater treatment, nitrate monitoring in food industry and also for "smart agriculture" purposes by determining the average nutrient status and variability in a field, thus enabling adjusted fertilizer application.

Environmental impact

It is now well known that the nitrate drained from the drainage network in U.S. mid-west farmlands might be responsible for the hypoxia seen in the northern Gulf of Mexico and Mississippi river. Currently, most environmental observations are under sampled as there is a long process of sample collection and then analysis in distant laboratories. Hence, wireless and sensor networks can be used in agricultural and environmental applications to study ions (*e.g.* nitrate and phosphate) uptake and run-offs. We have reported the design, fabrication and testing of a low cost, miniaturized and sensitive electrochemical sensor and sensor network for quantitative determination of nitrate ion concentrations in ground water samples to enable long-term high frequency monitoring of the environment.

Conventional bench-top nitrate analysis techniques, such as UV/Vis spectrometry, chromatography, HPLC and capillary electrophoresis,[14] are unsuitable for large-scale field deployment due to their massive instrumentation, bulky features, complex measurement procedures, and above all, cost. Commercial field nitrate sensors such as the YSI nitrate sensor (www.ysi.com) use ion-selective electrodes for its nitrate sensor. As we will show later, the detection limit of the YSI nitrate sensor at 142.5 μM is much higher than our reported value (0.4 μM) and our reported sensor is fabricated with a much lower cost. Other sensors like EcoLAB (http://www.envirotechinstruments.com) and SUNA (http://www.satlantic.com) use a UV optical based system, which are bulky compared to our microsensor. Another class of sensors, such as electrochemical biosensors, perform nitrate monitoring by exploiting enzymatic electrocatalytic processes.[15–18] In this electrochemical based sensor the reduction reaction is performed electrochemically by using suitable redox mediators (such as methyl viologen) which give rise to an amperometric signal. Further enzymatic colorimetric sensors have also been developed in which the enzymes such as nitrate reductase converts nitrate into nitrite, which in turn reacts with color reagents (Griess reaction) to form a pink color enabling colorimetric sensing. Such colorimetric based sensors are available commercially, for example, an analytical kit developed by NEC (http://www.nitrate.com/). However, the currently available nitrate sensors are not suitable for sensor network deployment. Due to simplicity, sufficient sensitivity and cost effectiveness, electrochemical based nitrate detection methods can be a viable option for sensor network deployments.[19] However, due to slow kinetics of charge transfer,[20] direct reduction of nitrate on bare metallic surfaces (Pt, Pd, Ru, Rh, Ir, Cu, Ag and Au) has limited applications. Among all the coinage metals studied so far[21,22] silver shows highest sensitivity for nitrate ion reduction in acidic or basic media.[23] In general, the sensitivity of a detection process strongly depends on the reaction kinetics as well as effective conduction of the electrons produced (due to oxidation or reduction) in the sensing device. Hence, a microscale device will be more sensitive compared to a macroscale.[24]

Wireless and sensor networks can be used in agricultural and environmental applications to study nitrate uptake and run-off. In this paper, we report the design, fabrication and testing of a low cost, miniaturized and sensitive electrochemical based nitrate sensor for point-of-care quantitative determination of nitrate in ground water samples. We also report the integration of the sensor into a wireless network and field water testing using the sensor. We use solid metal working electrodes for our sensor instead of a non-metal electrode such as carbon or mercury drop or a surface-modified electrode (e.g. freshly deposited metal complexes,[25] catalytic metals,[26] or immobilized biological catalysts[27]). The reasons for our preference for a solid metal electrode are as follows: it is compatible with micro-fabrication, it is straightforward to adapt the same fabrication to macro-scale and micro-scale sensors, it is feasible for surface regeneration if contaminated and, more importantly, it can be easily integrated with microelectronics and wireless radio for remote automated sensing.

Conceptual design of a sensor network

It is envisaged that a large number of distributed sensors (forming a sensor 'mesh') will continuously feed data into integration hubs, where data aggregation, correlation identification as well as information extraction will be performed. Using the results of this analysis, actions can be taken on the environment – thus providing a cyber-physical control loop in the system. Although sensors can provide only nodal information, sensor data can be fit in hierarchical models. Fig. 1 shows the schematic of the Illinois Nitrate sensor (iNits). The sensor consists of a sensor interface (input and output parameter interface for the sensor), and a low-power processor and wireless communication device called "Imote2". Finally, the sensor network is connected to a computer server for network data analysis.

Experimental methods

Microfabrication of the sensor

The schematic and optical images of the iNits are shown in Fig. 2(a) and (b) respectively. A close up view of the sensor electrodes is also shown in the inset. The sensor chips were microfabricated on a glass substrate. The precleaned microscope glass slides (Fisher scientific) were thoroughly rinsed with water, acetone and isopropyl alcohol (IPA) three times. The slides were blow-dried with a nitrogen gun and immediately taken for photolithography. Fig. S1 (ESI†) shows the steps for the entire microfabrication process. The different metal electrodes are fabricated using a lift-off technique and are described in detail in Fig. S1.† After the photolithography step, a thin layer of silver (200 nm) deposited by e-beam evaporation (Temescal) was used as working and reference electrodes and gold (200 nm) was used as the counter electrode. For proper adhesion to the glass substrate, 20 nm of the titanium layer was deposited before the metal depositions. We adopt a concentric design for the working and counter electrodes to improve the uniformity of current distribution between electrodes. The geometric area of the working electrode is 7.05×10^{-4} cm^2, the counter electrode has an area of 9.05×10^{-4} cm^2 and the area of the reference electrode is 3.47×10^{-4} cm^2. In order to minimize uncompensated ohmic loss, the reference electrode is kept close to the working electrode.

Miniaturized potentiostat design

In order to realize a wireless sensor network, not only the sensor itself but also the electrochemical potentiostat needs to be portable, easily implementable and low-cost. Moreover, the circuit design must have low power consumption to achieve long duration usage. Fig. S2 (see ESI†) illustrates the
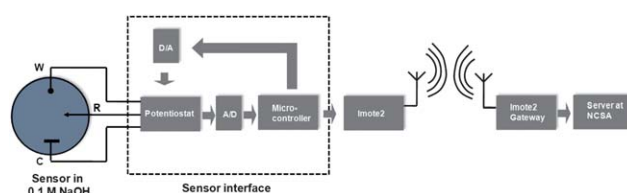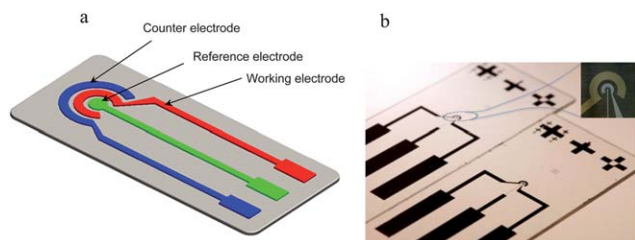

Fig. 1 Schematic of the sensor interface and communication system.

Fig. 2 Microfabrication of the sensor. (a) Schematic of the three electrode system of the nitrate microsensor. (b) Optical image of the microsensor.

schematic of the portable potentiostat circuit when connected to an Imote2 node and iNits. It is comprised of two operational amplifiers: The first (amplifier A) is combined with the iNits and a negative close loop. The output of operational amplifiers (OPA) provides current to maintain the voltage value set by Imote2 during electrochemical sensing. The other amplifier (amplifier B) is a trans-impedance amplifier. It converts current signal into voltage signal, which can be measured by a sensor board designed for data acquisition (SHM-DAQ). Moreover, a DC–DC power converter and D2A are utilized to provide appropriate power supply for amplifiers and analog signals.

With this schematic, one can send commands from the server and wirelessly control the remote Imote2 node to provide a bias and a triangular voltage signal. Then, the bias and triangular voltage are transmitted through the potentiostat circuit board and feed the desired value to the reference and working electrodes respectively. The bias signal at the working electrode acts as a virtual "ground" here and, as a result, an offset can be added to the triangular signal at the reference electrode, resulting in the desired negative or positive sweeping range. Since the potentiostat circuit is composed of a few active electronic devices, the price and power consumption is low compared to bulky commercial potentiostats. Fig. 3 shows the results obtained from the miniaturized potentiostat circuit. These results show that the performance of the miniaturized potentiostat is similar to that obtained from the commercial potentiostat. Any differences can be resolved through calibration. The inset of Fig. 3 also shows the potentiostat circuit board.
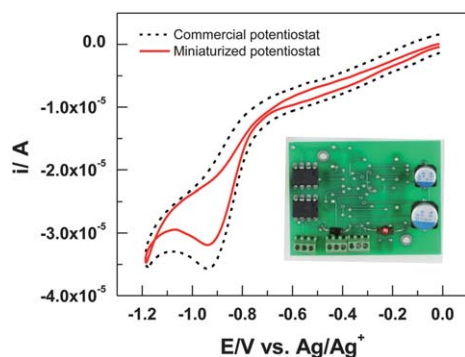
Results and discussion

In this section, we compare the performance of the typical macroelectrode (Ag wire of 0.5 mm diameter) with that of the fabricated microsensor. We have compared the performance in terms of reduction current density, sensitivity and reduction kinetics. We have also carried out an experiment to probe the effect of oxygen on the sensitivity of microsensors. The range and detection limit of the microsensor (iNits) is deduced from the calibration curve. Finally, the sensor has been tested with several water samples (tap water, lake water, bottled water, bored well, pond, stream water and ground water) to quantify the nitrate-nitrogen present in the sample. The results are also compared with the data obtained from the enzymatic nitrate reductase, ultraviolet spectrophotometric screening, ion selective electrodes, cadmium reduction as well as colorimetric detection study.

A typical nitrate (NO_3^-) reduction follows a two electron transfer process to form nitrite as shown in eqn (1):[21,28–30]
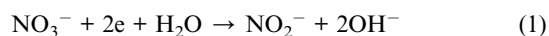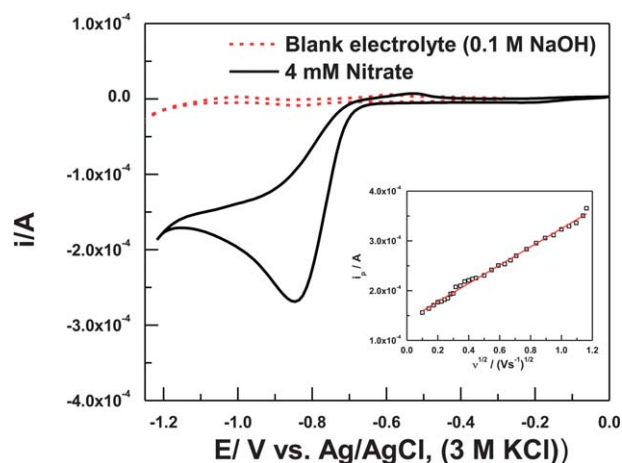
$$NO_3^- + 2e + H_2O \rightarrow NO_2^- + 2OH^- \quad (1)$$

Fig. 4 shows a typical cyclic voltammetry (CV) recorded using an Ag wire electrode (macroelectrode) in 4 mM $NaNO_3$ and 0.1 M NaOH (pH = 13) at a scan rate of 50 mV s^{-1}. Alkaline electrolytes with a high pH value help to shift hydrogen evolution towards more negative potentials in comparison to nitrate reduction[22,29] and, consequently, allow for a well-defined nitrate reduction wave. The cathodic peak at −0.9 V is due to the reduction of nitrate ions. The peak current decreases appreciably with repetitive voltage sweep, indicating nitrate depletion. The linear relationship between the peak current (i_p) and the square root of the scan rate ($v^{1/2}$) (Fig. 4, inset) indicates that the rate limiting step of the electroactive species is diffusion controlled. The diffusion coefficient for the reaction can be calculated from eqn (2):[31]

$$i_p = 2.99 \times 10^5 (\beta \times n)^{1/2} A D^{1/2} v^{1/2} C^* \quad (2)$$

where β is the cathodic transfer coefficient, n is the number of electrons involved in the limiting step reaction, A is the electrode

Fig. 3 Comparison of CV obtained from a commercial potentiostat and miniaturized potentiostat for 10 mM nitrate in 0.1 M NaOH solution (50 mV s^{-1}).

Fig. 4 Typical voltammograms (0.05 V s^{-1}) showing nitrate reduction for 4 mM solution in 0.1 M NaOH electrolyte using a silver macroelectrode.

area (cm^2), D is the diffusion coefficient (cm^2 s^{-1}), and C^* is the concentration of NO$_3^-$ in the solution (mol cm^{-3}). $\beta \times n$ can be calculated from eqn (3)

$$E_p - E_{p/2} = \frac{47.7}{\beta \times n} \quad (3)$$

where E_p is the peak potential (V) and $E_{p/2}$ is the potential where $i = i_p/2$ (A). For a nitrate concentration of 10 mM and a scan rate of 0.05 V s^{-1}, $\beta \times n$ and D are calculated to be 0.65 and 8.99 $\times$ 10^{-6} cm^2 s^{-1} respectively. Strictly speaking, eqn (3) and hence the calculation of $\beta \times n$ and D are valid only when the voltammetric process is irreversible and E_p is fairly invariant with scan rates.

The negative shift of the peak potential (E_p) with an increasing scan rate (0.01 to 1.35 V s^{-1}) using the macroelectrode (see ESI, Fig. S3†) demonstrates that the electron transfer in the reduction reaction is an irreversible process. The anodic peak at −0.55 V (prominently seen for a higher scan rate) is generally attributed to hydroxide electrochemisorption (electrosorption with charge transfer).[32,33] The magnitude of $E_p - E_{p/2}$ was in the range of 60 to 95 mV, indicating that electron transfer is the rate determining step.[34] In addition, the function $i_p/v^{1/2}$ decreased monotonously (ESI, Fig. S4†) with $v^{1/2}$ which is an indication that the chemical reaction is coupled with the electron transfer.[31] The variation of $i_p/v^{1/2}$ with the scan rate also suggests that nitrate ion reduction does not follow a normal Butler–Volmer kinetics.[29] In order to compare the sensitivity of microsensors with macroelectrodes in the current study as well as in the literature (Table 1), we have defined a normalized sensitivity, $\overline{i_p}$, as:

$$\overline{i_p} = \frac{i_p}{nAv^{1/2}C^*}\left(\frac{\text{A s}^{1/2}}{\text{V}^{1/2}\,\text{M cm}^2}\right) \quad (4)$$

where n is the number of electrons in the reduction step (=2), A is the surface area of the electrode (cm^2), v is the sweep rate for the potential (V s^{-1}), and C^* is the concentration of nitrate in the solution (M). Interestingly, the microsensor electrode showed greater sensitivity compared to what is commonly reported in the literature (Table 1); the only exception is the work by Lundquist et al.,[35] where a complex agent, LaCl$_3$ was included in the electrolyte. The CV recorded using a microsensor in 10 mM nitrate and 0.1 M NaOH electrolyte with varying the scan rates from 10 to 1350 mV s^{-1} is shown in Fig. 5. The microsensor showed

higher current density than that obtained by the macroelectrode for the same concentration (compare with Fig. S3, see ESI†). The inset of Fig. 5 also shows the peak potential vs. scan rate, indicating that the reduction reaction is irreversible. Similarly, Fig. S5 (ESI†) shows the variation of $i_p/v^{1/2}$ against the scan rate for nitrate reduction using a microsensor in 0.1 M NaOH electrolyte, indicating a deviation from Butler–Volmer kinetics. It should be noted that eqn (2)–(4) were derived for the disk electrodes. Although our geometry is not disk-like, we still use these equations for the wire electrode and for the iNits geometry as done in literature for many untested geometries.[22] Further analysis of the nitrate reduction process and comparison with the bond dissociation free energy has been presented in the ESI.†

Effect of oxygen ingression

Since the sensor will be placed in the field where a controlled environment like in the laboratory is not possible, we want to quantify the effect of oxygen ingression. The effect of oxygen ingression on the sensitivity of a nitrate sensor was probed by intentionally admitting oxygen into the solution. Air saturated
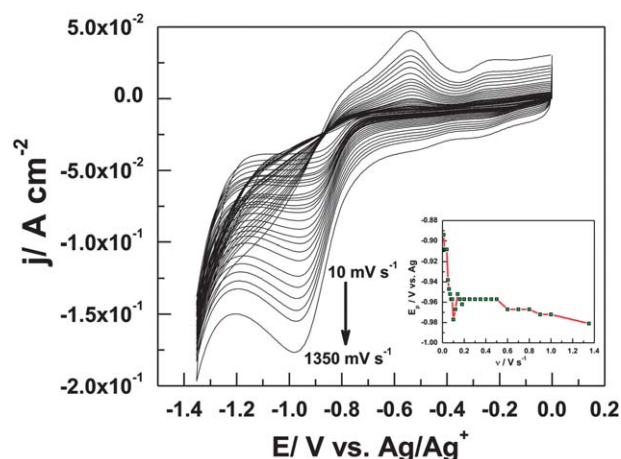

Fig. 5 Cyclic voltammograms using a microsensor in 10 mM NO$_3^-$ and 0.1 M NaOH, with varying the scan rate from 10 to 1350 mV s^{-1}. Inset shows the variation of peak potential vs. scan rate.

Table 1 Normalized peak current for reduction of nitrate

$\overline{i_p}\left(\dfrac{\text{A s}^{1/2}}{\text{V}^{1/2}\,\text{M cm}^2}\right)$	v/V s^{-1}	A/cm^{-2}	Supporting electrolyte	Electrode	Reference
5.52	0.01	7.05 × 10^{-4}	0.1 M NaOH	Silver (iNits)	This work
0.582	0.01	0.11	0.1 M NaOH	Silver wire	This work
2.47	0.01	0.00196	0.01 M NaOH	Silver disk	22
1.3	0.002	1.2	0.5 M H$_2$SO$_4$ + 0.1 mM KCl + 0.01 M CuSO$_4$	Copper-plated graphite	36
0.43	0.01	18	0.1 M Na$_2$SO$_4$ + 0.1 M HCl	Copper-plated glassy carbon	37
0.77	0.1	0.196	0.1 M NaH$_2$PO$_4$ + 10 μM CdCl$_2$ + 50 μM CuCl$_2$	Copper/cadmium-plated pyrolytic graphite	38
14	0.01	0.034	0.1 M KCl + 0.01 M LaCl$_3$	Hanging mercury drop	35
2.08	0.005	0.2826	0.5 M H$_2$SO$_4$	Graphite modified doped-polypyrrole nanowire	39
0.79	0.1	0.07	0.1 M NaSO$_4$ (pH = 2.0, H$_2$SO$_4$)	Copper wire	40
3.55	0.05	0.01	0.1 M NaSO$_4$ (pH = 3.0, H$_2$SO$_4$)	Copper-plated platinum microelectrode	41

aqueous solution contains about 0.3 mM of oxygen.[42] Oxygen reduction takes place in alkaline media as follows:

$$O_2 + 2H_2O + 4e^- \rightarrow 4OH^-$$
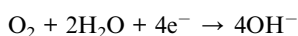
Oxygen reduction takes place at a more positive potential than nitrate reduction and hence, large current from the oxygen reduction interferes with the nitrate measurement. Fig. S6 (ESI†) shows a typical cyclic voltammogram (50 and 100 mV s^{-1}) for the reduction of 4 mM nitrate in 0.1 M NaOH electrolyte with and without oxygen purging respectively using a macroelectrode (silver wire electrode). We observed a substantial decrease in the reduction current without oxygen purging.

Calibration curve

In order to test the microsensors, a polydimethylsiloxane (PDMS) based microfluidics chamber was prepared for the sensor to hold the sample. Fig. S7† shows the cyclic voltammetry (CV) curve of nitrate with different concentrations using the microsensor in microfluidics. The calibration curve for nitrate reduction using the microsensor is shown in Fig. S8.† Known nitrate concentrations of 0.5 nM to 50 mM were prepared from the nitrate stock solution. The relationship between the cyclic voltammetry peak current and the concentration of nitrate was investigated using regression analysis. We find that the calibration curve shows three different responses in three ranges: (1) non-linear from 0.5 nM to 5 µM, with the equation $(-I_p/A) = 1.63 \times 10^{-6} - 5.29 \times 10^{-7}\exp[-(C_{nitrate}/mol\ L^{-1})/7.04 \times 10^{-7}]$, (2) linear response from 5 µM to 500 µM with the equation $(-I_p/A) = 1.58 \times 10^{-6} + 0.00605(C_{nitrate}/mol\ L^{-1})$, and (3) linear response from 500 µM to 50 mM with a different slope, with the resulting equation $(-I_p/A) = -3.26 \times 10^{-7} + 0.00154(C_{nitrate}/mol\ L^{-1})$. The correlation coefficient R^2 is more than 0.999 in all the cases. The detection (3 SD) and quantification (10 SD) limits are estimated at 0.4 µM (25 ppb) and 1.33 µM (83 ppb), respectively. The figures of merit for the macroelectrode and the microsensor electrode are summarized in Table 2.

Measurement of nitrate in water samples

Fifteen different water samples such as tap water (Chicago; Urbana; Los Angeles; San Diego), lake water (Lake of the woods, Champaign county, Illinois; Crystal lake, Champaign; Michigan lake, Chicago), bottled water (Nestle pure life), bored well (Champaign, Illinois), pond water (Lake of the woods, Champaign county, Illinois), stream water (Champaign, Illinois), and spring water (South campus, University of Illinois at Urbana-Champaign) were collected. The location of the water samples collected is shown on google-map in Fig. S9.† The

microsensor was utilized to determine the nitrate concentration in the collected water samples. The resulting CV is shown in Fig. S10 and S11.† The nitrate concentration was calculated using the calibration curve obtained earlier and the nitrate-nitrogen amounts detected in the water samples are close to 0.7–1.2 ppm.

Further, we utilized the enzymatic nitrate reductase method, ultraviolet (UV) absorption spectroscopy, second derivative UV screening, ion selective electrodes, a cadmium reduction method and a colorimetric detection method to detect and independently compare the nitrate-nitrogen concentration for all water samples obtained using the electrochemical method. The water quality data of all tested water samples are provided in Table S1.† Briefly, the water quality data ranges are as follows: pH = 7.0–8.4, total hardness = 100–500 ppm, total chlorine = 0.0–1.0 ppm, and total alkalinity = 80–240 ppm. Nitrate reductase (NaR) is an enzyme based nitrate analysis method,[15–18] where nitrate is reduced to nitrite using a nitrate reductase NADH (nicotinamide adenine dinucleotide). The nitrite is then reacted with color reagents such as sulfanilamide and N-naphthylethylenediamine (NED) (Griess assay) to form a pink color easily detected by the naked eye or photodetectors. For the experiment we used the commercially available nitrate test kits (www.nitrate.com) (Fig. S12†). In the cadmium reduction methods, instead of the enzyme, cadmium is used to reduce nitrate to nitrite followed by a Griess assay (sulfanilic acid, gentisic acid and chromotropic acid) to form a detectable color. In the ultraviolet (UV) absorption spectroscopy (Evolution 60 UV-Visible Spectrophotometer) method, a quartz cuvette containing the liquid sample was tested by scanning wavelength in the range from 190 nm to 450 nm, with a scanning step of 1 nm. The nitrate concentrations in the water samples were determined from the calibration curve obtained using a known concentration of nitrate standards (Fig. S13–S15†). The details of the experiments are provided in the ESI.† In order to minimize the possible interference from dissolved organic matter (DOM), which usually have a UV absorbance peak from 200–240 nm, we have also performed a second derivative of the nitrate curve to eliminate the interferences that are linear. The nitrate concentrations in the water samples were determined from the calibration curve obtained from the second derivative curve of known concentration of nitrate standards (Fig. S16†). Fig. 6 shows the comparison of different nitrate methods to determine the nitrate-nitrogen concentration in water samples. The concentration of water samples is in the range of 0–8 ppm nitrate-nitrogen. The results from electrochemical sensors match well with the cadmium reduction method (which is usually the gold-standard for determination of nitrate concentration).

Wireless sensor network

Wireless Smart Sensor Networks (WSSNs) facilitate empirical observation and evaluation of the holistic environmental system, thus enabling inexpensive sensing, communication, and computational capabilities. A number of wireless smart sensor networks (WSSNs) are in use today to monitor some aspects of the environment; using data from these WSSNs, models are calibrated and operational decisions are made.[43–48] Dense sensor network deployments allow for effective observation and understanding

Table 2 Analytical parameters for nitrate reduction

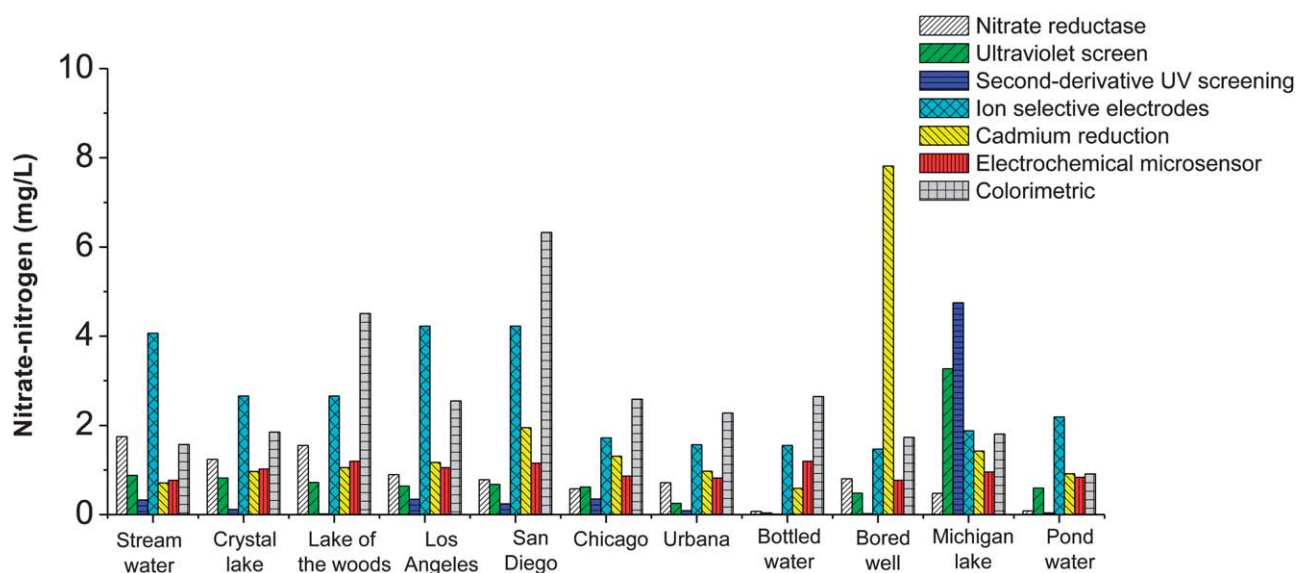| Analytical parameters	Macroelectrode	Microsensor
Sample volume (mL)	25	0.07
Detection limit (µM)	12	0.4
Quantification limit (µM)	40	1.33
Linear range (mM)	0.005–50	0.005–50

Fig. 6 Comparison of different nitrate methods to determine the nitrate-nitrogen concentration in water samples.

of emergent phenomena while improving the fault tolerance of a network. Using smart, inexpensive sensors, high spatial resolution can be achieved through dense deployment of sensor nodes,[49] which in turn promises improved fault tolerance in the network.

A typical smart sensor node has a microcontroller which performs basic processing operations, memory, a radio transceiver for wireless communication, transducers, a power source, and one or more sensors. The sensor boards used in our test bed can measure temperature, light, humidity, and connect to up to four external digital/analog sensors. Our smart sensor nodes consist of an Imote2 and a sensor board stacked on the Imote2 (Fig. 7(a)). The Imote2 is built around the Intel PXA271 processor (13–416 MHz) and has 256 kB of SRAM memory,

32 MB of SDRAM, and 32 MB of flash memory. It has an integrated 802.15.4 (ZigBee) radio, interfaces with USB and supports 3xUART, 2xSPI, I2C, SDIO, and GPIOs I/O standards. ZigBee is designed for short range communication but its range can be extended up to approximately 150 m by using more specialized antennas. The operating system on the Imote2 is TinyOS, which is a component-based operating system and a platform for wireless sensor networks.

Prior to deployment, the sensor nodes are programmed with software that provides network, application, and web services. The implemented software tool-suite provides customizable middleware services for WSN applications including multi-hop communication,[50] power management, data aggregation, reliable communication, and time synchronization. This leads to highly
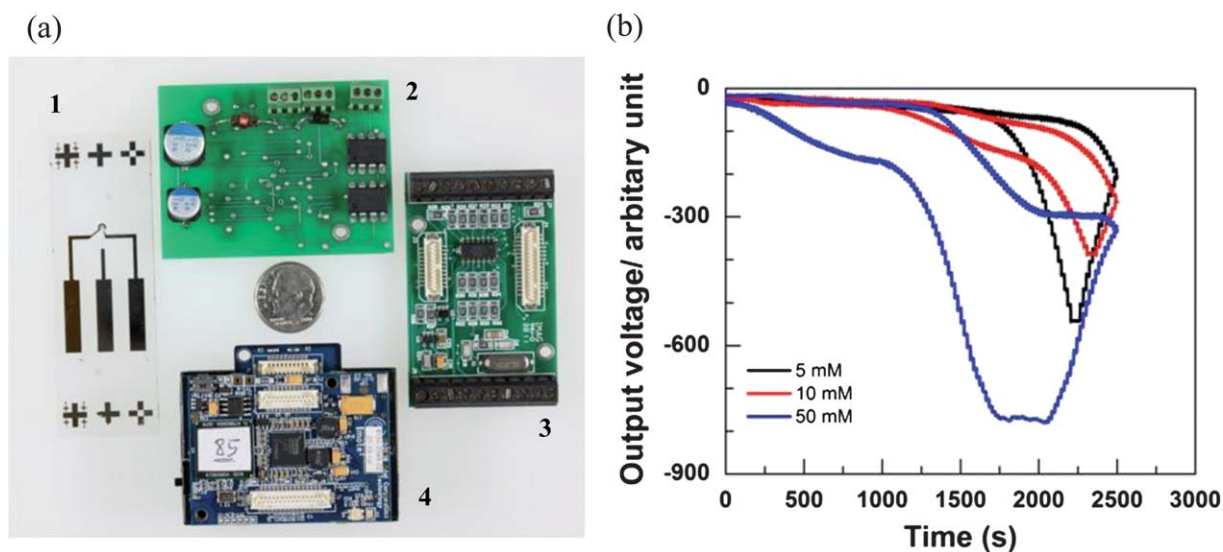

Fig. 7 (a) The integrated module: (1) iNits, (2) miniaturized PCB for potentiostat, (3) SHM-DAQ board, and (4) Imote2. (b) Demonstration of nitrate ion concentration measurements using the integrated module.

efficient services that can be used by diverse applications, in particular to provide adaptive sampling and data storage. Fig. 7(b) shows a demonstration in the lab with the Imote2 and sensor board measuring different nitrate concentrations. Once data is collected, it is transferred wirelessly to a laptop base station.

Given the geographic scale of the observation areas where the nitrate sensors could be deployed and the large number of potential events that need to be monitored, sensing resources will necessarily be limited and must be managed intelligently to achieve an acceptable level of network sensing performance. Keeping the smart sensor nodes on all the time is not feasible as they will run out of power within a few days if they are not put in low-power modes. The challenge is to get the desired spatio-temporal resolution in response to external events without expending the energy required to keep all the nodes continuously awake. A sentry service addresses this by selecting only a few nodes for high frequency sensing; these nodes can wake other nodes up to record data if an interesting event occurs. The implemented software tool-suite provides a hierarchical sensor control system that will manage the sensing processes and a sentry service[51] with the aim of reducing the energy consumption of the entire system. The sentry service divides the sensor nodes into three groups: gateway, sentry and leaf nodes. Gateway nodes are the relay nodes connected to a base station. Except for the gateway nodes all nodes are put in an energy saving sleep mode. The leaf nodes are scheduled to wake up and sample at regular and long intervals (*e.g.* a few times a day). The sentry nodes wake up more frequently and perform sensing. The role of the sentry nodes is to capture *interesting* events and wake up the network through the gateway node. In the event of a sudden change in the captured data or any other environmentally significant event, the sentry nodes send a signal to the gateway node which in turn signals the rest of the network and commands sensing and data retrieval.

Conclusions

In summary, we have performed the design, fabrication and testing of a low cost, miniaturized and sensitive electrochemical based nitrate sensor for quantitative determination of nitrate in a ground water sample. In order to enable remote operation and field deployment with a wireless interface, we designed, fabricated and tested a miniaturized potentiostat circuit. We have compared the performance of a microsensor with that of a macroelectrode-based electrochemical system. Rigorous analysis showed that the microsensor has higher sensitivity than conventional macroelectrodes. The limit of detection (LOD) for the microsensor was about 25 ppb (0.4 µM) and the limit of quantification (LOQ) was about 83 ppb (1.33 µM). The microsensor was used for the cyclic voltammetric determination of nitrate ions in several water samples. We compared the performance of the microsensor by testing the water samples using an enzymatic nitrate reductase method, ultraviolet (UV) absorption spectroscopy, second derivative UV screening, ion selective electrodes, a cadmium reduction method and a colorimetric detection method. Finally, the microsensor was successfully tested with wireless interface and miniaturized potentiostat in a lab environment for nitrate detection. The field deployment of the sensor network is underway.

References

1 J. Dechorgnat, C. T. Nguyen, P. Armengaud, M. Jossier, E. Diatloff, S. Filleur and F. Daniel-Vedele, *J. Exp. Bot.*, 2011, **62**, 1349–1359.
2 P. F. Swann, *Proc. R. Soc. Med.*, 1977, **70**, 113–115.
3 H. J. Di and K. C. Cameron, *Nutr. Cycling Agroecosyst.*, 2007, **79**, 281–290.
4 O. Bodansky, *Pharmacol. Rev.*, 1951, **3**, 144–196.
5 C. S. Bruningfann and J. B. Kaneene, *Vet. Hum. Toxicol.*, 1993, **35**, 521–538.
6 G. Ellis, I. Adatia, M. Yazdanpanah and S. K. Makela, *Clin. Biochem.*, 1998, **31**, 195–220.
7 C. L. Walters, *Oncology*, 1980, **37**, 289–296.
8 T. M. Addiscott, A. P. Whitmore and D. S. Powlson, *Farming, Fertilizers and the Nitrate Problem*, 1991.
9 Environmental Protection Agency, *List of Contaminants & Their Maximum Contaminant Level (MCLs)*, http://www.epa.gov/safewater/contaminants/dw_contamfs/nitrates.html.
10 A. J. Miller, X. Fan, M. Orsel, S. J. Smith and D. M. Wells, *J. Exp. Bot.*, 2007, **58**, 2297–2306.
11 P. L. Altman and D. S. Dittmer, *Environmental Biology*, 1966.
12 J. D. Wolt, *Soil Solution Chemistry: Applications to Environmental Science and Agriculture*, 1994.
13 K. S. Johnson, J. A. Needoba, S. C. Riser and W. J. Showers, *Chem. Rev.*, 2007, **107**, 623–640.
14 M. J. Moorcroft, J. Davis and R. G. Compton, *Talanta*, 2001, **54**, 785–803.
15 L. M. Moretto, P. Ugo, M. Zanata, P. Guerriero and C. R. Martin, *Anal. Chem.*, 1998, **70**(10), 2163–2166.
16 S. A. Glazier, E. R. Campbell and W. H. Campbell, *Anal. Chem.*, 1998, **70**, 1511–1515.
17 D. Quan, J. H. Shim, J. D. Kim, H. S. Park, G. S. Cha and H. Nam, *Anal. Chem.*, 2005, **77**, 4467–4473.
18 S. Cosnier, S. Da Silva, D. Shan and K. Gorgy, *Bioelectrochemistry*, 2008, **74**, 47–51.
19 D. Kim, I. B. Goldberg and J. W. Judy, *Sens. Actuators, B*, 2009, **135**, 618–624.
20 G. E. Dima, A. C. A. de Vooys and M. T. M. Koper, *J. Electroanal. Chem.*, 2003, **554**, 15–23.
21 J. Krista, M. Kopanica and L. Novotny, *Electroanalysis*, 2000, **12**, 199–204.
22 D. Kim, I. B. Goldberg and J. W. Judy, *Analyst*, 2007, **132**, 350–357.
23 V. Rosca, M. Duca, M. T. de Groot and M. T. M. Koper, *Chem. Rev.*, 2009, **109**, 2209–2244.
24 Y. Xiao, F. Patolsky, E. Katz, J. F. Hainfeld and I. Willner, *Science*, 2003, **299**, 1877–1881.
25 Z. M. Liu, X. D. Xi, S. J. Dong and E. K. Wang, *Anal. Chim. Acta*, 1997, **345**, 147–153.
26 N. G. Carpenter and D. Pletcher, *Anal. Chim. Acta*, 1995, **317**, 287–293.
27 L. H. Larsen, T. Kjaer and N. P. Revsbech, *Anal. Chem.*, 1997, **69**, 3527–3531.
28 S. Cattarin, *J. Appl. Electrochem.*, 1992, **22**, 1077–1081.
29 M. A. Bhat, P. P. Ingole, V. R. Chaudhari and S. K. Haram, *New J. Chem.*, 2009, **33**, 207–210.
30 K. Fajerwerg, V. Ynam, B. Chaudret, V. Garcon, D. Thouron and M. Comtat, *Electrochem. Commun.*, 2010, **12**, 1439–1441.
31 A. J. Bard and L. R. Faulkner, *Electrochemical Methods: Fundamentals and Applications*, Wiley, New York, 2001.
32 E. R. Savinova, P. Kraft, B. Pettinger and K. Doblhofer, *J. Electroanal. Chem.*, 1997, **430**, 47–56.
33 E. R. Savinova, S. Wasle and K. Doblhofer, *Electrochim. Acta*, 1998, **44**, 1341–1348.
34 C. P. Andrieux and J. M. Saveant, in *Investigations of Rates and Mechanisms of Reactions*, ed. C. F. Bernasconi, Wiley, New York, Part 2 edn, 1986, vol. VI/4E.
35 G. L. Lundquist, G. Washinger and J. A. Cox, *Anal. Chem.*, 1975, **47**, 319–322.
36 A. G. Fogg, S. P. Scullion, T. E. Edmonds and B. J. Birch, *Analyst*, 1991, **116**, 573–579.
37 J. Davis, M. J. Moorcroft, S. J. Wilkins, R. G. Compton and M. F. Cardosi, *Analyst*, 2000, **125**, 737–741.
38 M. E. Bodini and D. T. Sawyer, *Anal. Chem.*, 1977, **49**, 485–489.

39 X. L. Zhang, J. X. Wang, Z. Wang and S. C. Wang, *Sensors*, 2005, **5**, 580–593.
40 T. R. L. C. Paixao, J. L. Cardoso and M. Bertotti, *Talanta*, 2007, **71**, 186–191.
41 Y. Li, J. Sun, C. Bian, J. Tong and S. Xia, *Procedia Eng.*, 2010, **5**, 339–342.
42 C. Colombo and C. M. G. van den Berg, *Anal. Chim. Acta*, 1998, **377**, 229–240.
43 S. Anumalla, B. Ramamurthy, D. Gosselin and M. Burbach, *IEEE International Conference on Electro Information Technology*, 2005.
44 M. Britton and L. Sacks, *The SECOAS Project: Development of a Self-organizing, Wireless Sensor Network for Environmental Monitoring, SANPA-2004*, pp. 1–7.
45 M. Jiang, Z. Guo, F. Hong, Y. Ma and H. Luo, *Oceansense: A Practical Wire- Less Sensor Network on the Surface of the Sea, PerCom-2009*, 2009.
46 D. C. Steere, A. Baptista, D. McNamee, C. Pu and J. Walpole, *Research Challenges in Environmental Observation and Forecasting Systems, MobiCom-00*, 2000, pp. 292–299.
47 Y. Xiao, J. Zhang, T. Liu and X. Ga, *An Environmental Monitoring System Based on Zigbee for Emergency Applications, WiCOM-2009*, 2009.
48 D. Diamond, S. Coyle, S. Scarmagnani and J. Hayes, *Chem. Rev.*, 2008, **108**, 652–679.
49 A. Mainwaring, D. Culler, J. Polastre, R. Szewczyk and J. Anderson, *Wireless Sensor Networks for Habitat Monitoring, WSNA-02*, 2002, pp. 88–97.
50 T. Nagayama, P. Moinzadeh, K. Mechitov, M. Ushita, N. Makihata, M. Ieiri, G. Agha, B. F. Spencer, Y. Fujino and J.-W. Seo, Reliable multi-hop communication for structural health monitoring, *Smart Structures and Systems*, 2010, **6**, 481–504.
51 J. Rice, K. Mechitov, B. F. Spencer and G. Agha, Autonomous smart sensor network for full-scale structural health monitoring, *Proc. SPIE Smart Structures/NDE*, 2010, **7647**.